Editors' Suggestion

Tokamak Plasmas with Density up to 10 Times the Greenwald Limit

N. C. Hurst,* B. E. Chapman, J. S. Sarff, A. F. Almagri, K. J. McCollam, D. J. Den Hartog, J. B. Flahavan, and C. B. Forest
Department of Physics, University of Wisconsin - Madison, Madison, Wisconsin, USA

(Received 12 January 2024; accepted 3 June 2024; published 29 July 2024)

Current-carrying, toroidal laboratory plasmas typically cannot be sustained with an electron density above the empirical Greenwald limit. Presented here are tokamak experiments in the Madison Symmetric Torus with a density up to an unprecedented level about 10 times this limit. This is thought to be made possible in part by a thick, stabilizing, conductive wall, and a high-voltage, feedback-controlled power supply driving the plasma current. The radial profile of the toroidal current flattens around twice the limit, without the edge collapse routinely observed in other experiments.

DOI: 10.1103/PhysRevLett.133.055101

Toroidal plasma experiments routinely encounter operational limits on the electron density, n_e, above which they cannot be sustained [1,2]. In the tokamak and reversed-field pinch configurations where confinement relies on current, I_p, flowing in the plasma, empirical results from a wide database of experiments follow a simple formula known as the Greenwald density limit: $n_G = I_p[\mathrm{MA}]/\pi a^2$, where n_G is the line-average electron density through the plasma core in units of 10^{20} m^{-3}, and a [m] is the plasma minor radius [3,4]. This imposes a strong constraint on nuclear fusion power production, which scales as density squared [5]. ITER, SPARC, and other future reactor-scale tokamaks may need to operate with Greenwald fraction $f_G = n_e/n_G$ near or above unity, highlighting the importance of understanding density limit physics [6,7].

Despite the simplicity of the Greenwald formula, a striking consistency across a wide range of experiments, and a large volume of research on the topic, the mechanism(s) underlying the limit is not well understood [4,8–13]. It is widely agreed that radiative power balance is involved, due to the strong scaling of plasma radiative cooling with density [14] and increased radiation measured in many experiments as the limit is approached [15,16]. Typically, the edge pressure profile collapses near the limit, which increases the local resistivity and stops current from flowing, such that the plasma detaches from the wall or separatrix and shrinks radially. This sets up an unstable current gradient that causes a global, catastrophic loss of confinement known as a disruption. Interestingly, the limit can be exceeded up to $f_G \sim 1.5$ when strongly peaked density profiles are prepared, supporting the idea that the limit is governed by plasma edge physics [17,18]. Various theoretical models have been put forward to explain the edge pressure collapse that is central to density limit behavior, many of which invoke other forms of transport or energy loss beyond simple radiative cooling. These include radiation-destabilized tearing modes [10,19], interchange or ballooning turbulence [12,20], and weakened shear layers [21]. Recent studies suggest that the density limit for high-confinement (H-mode) tokamak plasmas depends on input power [13,22], which does not appear in n_G and is a key parameter for density limits in stellarator devices that do not carry substantial plasma current [23].

Presented here are tokamak experiments with an electron density exceeding the Greenwald limit by up to a factor of 10 in steady conditions, which is unprecedented. The maximum density appears to be set by hardware limitations rather than plasma instability. The experiments are conducted in the Madison Symmetric Torus (MST) device [24], operated as a tokamak with toroidal field $B_\phi = 0.13$ T, $I_p = 50$ kA, and major/minor radius $R_0/a = 1.5/0.52$ m. Line-averaged electron densities ranging up to about $6 \times 10^{19}\mathrm{m}^{-3}$ are measured by an interferometer. Internal magnetic probe measurements indicate that the toroidal current profile remains finite up to the limiter and globally flattens around $f_G = 2$, in contrast with the edge collapse observed in other devices. Density scalings of input power and impurity radiation increase sharply at n_G, indicating that a Greenwald-like mechanism, similar to that observed in other devices, may be active even though it does not cause disruption. Measurements of total radiated power, temperature, flows, and impurity content are not presently available. The capability of operation at high f_G is thought to be associated with two unique features of MST: a thick, close-fitting, conductive wall that stabilizes magnetohydrodynamic fluctuations near the plasma edge; and a high-loop-voltage power supply that can drive current through low-temperature, resistive plasma at high density. The results presented here offer insight into models of density-limit physics, enable studies of a new regime of high-normalized-density tokamak plasmas, and may help

*Contact author: nhurst@wisc.edu

future tokamaks to exceed operational density limits and/or avoid disruptions.

The MST is a toroidal device that was primarily designed and used for reversed-field pinch plasmas [24] and has recently been operated as an ohmically heated tokamak with several unique features, including the unusual ability to operate nondisruptively with edge safety factor $q(a) < 2$ [25]. The plasma is surrounded by a circular cross-section, 5-cm-thick aluminum shell with inner radius $a = 0.52$ m, and graphite limiters at radius 0.5 m. The resistive wall time is $\tau_w = 800$ ms, much longer than the typical discharge duration of 50 ms. This inhibits the growth of resistive wall modes (RWM) during the discharge, and may impact the growth of internal tearing modes [26]. The toroidal magnetic field is created by driving current directly through the shell as a single-turn loop. Because of the low toroidal field and lack of auxiliary heating, the electron temperature is presently limited to $T_e < 100$ eV in MST tokamak plasmas. In comparison, other modern, high-performance tokamaks have $T_e \sim 10$ keV and thus lower collisionality and resistivity by several orders of magnitude.

The plasma current is driven inductively by either of two separate power supplies: a *passive* pulse-forming network consisting of staged capacitor bank discharges, or an *active* feedback-controlled programmable power supply that dynamically adjusts its output voltage to meet an arbitrary demand waveform for the transformer primary current [27]. This Letter focuses on plasmas driven by the active supply, but plasmas driven by the passive supply are discussed briefly for comparison. For all discharges driven by the active supply, a flattop current $I_p = 55$ kA is programmed, corresponding to $q(a) = 2.2$. The working gas is deuterium injected with wall-mounted puff valves.

A set of tokamak discharges driven by the active power supply are presented in Fig. 1 with f_G ranging from about 0.5 to 10. The density is measured using an interferometer chord passing approximately through the magnetic axis, which is one of 11 chords spanning the plasma diameter [28]. The loop voltage increases with f_G from about 3 to 65 V as the feedback system attempts to meet the plasma current demand in increasingly resistive conditions. At higher densities, I_p decreases over time to around 45–50 kA as the power supply fails to meet the demand. For $f_G > 5$, the demand waveform was changed to include a slight ramp-up in an attempt to flatten the plasma current waveform. At the highest densities, the discharges terminate earlier than the programmed I_p ramp-down at 40 ms. This is due to consumption of the available 2 V-s flux swing in the iron-core poloidal field transformer, which is associated with high plasma resistivity and sets the maximum density.

To better understand the role of the active power supply in exceeding the Greenwald limit, plasmas with $I_p \sim 50$ kA were studied using the passive supply. Figure 2(a) shows such a discharge with f_G near unity, which ended due to a

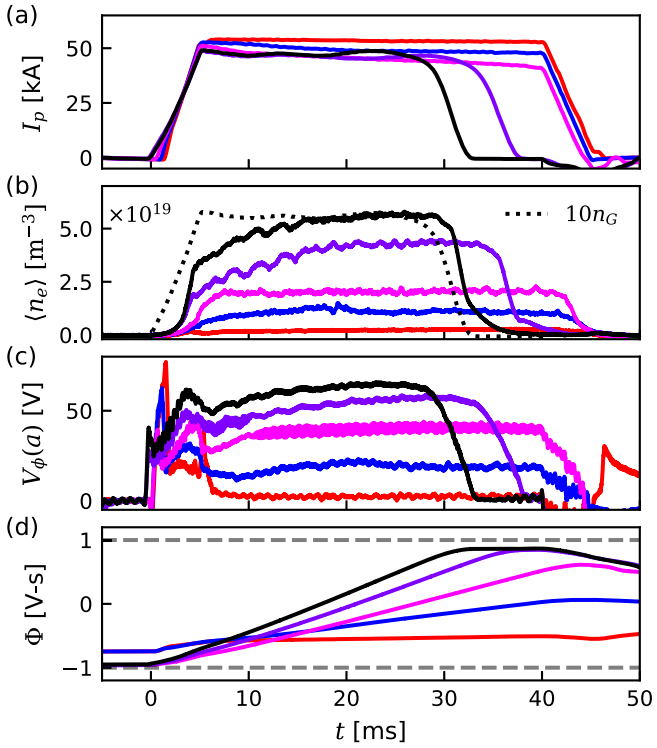

FIG. 1. Tokamak discharges driven by the active power supply with normalized density, f_G, ranging from 0.5 to 10. (a) Plasma current; (b) line-averaged electron density measured by an interferometer, and $10n_G$ (dotted line) calculated from the plasma current waveform in the highest density discharge; (c) surface toroidal voltage, equal to the loop voltage in steady state; and (d) flux in poloidal field transformer, where the available range is given by dashed lines.

programmed toroidal field ramp-down at $t = 45$ ms. A separate discharge in panel (b) exceeded n_G significantly, causing early termination. However, there was no evidence of strong instabilities or rapid current quench, which are characteristic of disruptive behavior. The passive power supply is designed to apply large loop voltage during start up and smaller voltage throughout the discharge, and is therefore unable to sustain I_p in conditions of high density and resistivity. Thus, operation with $f_G > 1$ is only possible using the active power supply, so henceforth only this case is discussed.

The scalings of several measured quantities with plasma density are shown in Fig. 3, where averages are taken over $20 < t < 30$ ms during the plasma current flattop. Two datasets span $0.8 < f_G < 3$ with the power supply capacitance $C = 84$ mF (a measure of stored energy), one of which had a probe inserted up to 20 cm into the plasma. Another dataset spans $0.4 < f_G < 10$ with C doubled to 168 mF and a probe inserted to 10 cm depth. Panel (a) shows the ohmic input power, $P_{\text{ohm}} = I_p V_{\text{loop}}$, where the increase with density is largely associated with V_{loop} since I_p is held in the range 45–55 kA. Panel (b) shows corresponding measurements of radiation from a

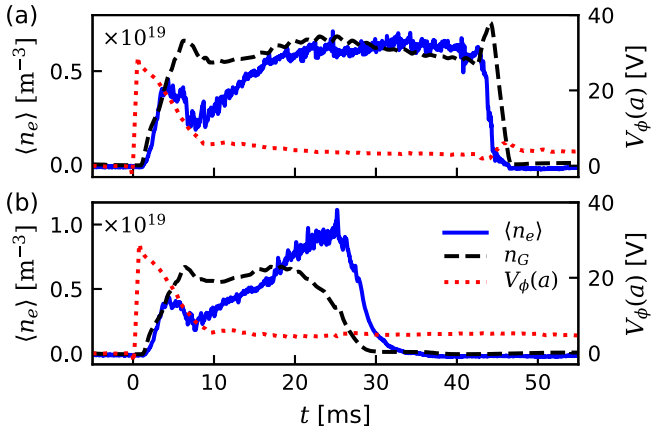

FIG. 2. Two tokamak discharges (a),(b) with plasma current driven by the passive power supply, including line-average density $\langle n_e \rangle$ (blue), Greenwald density n_G (black, dashed), and surface toroidal voltage $V_\phi(a)$ (red, dotted), where discharge (b) terminates when $n_e > n_G$.

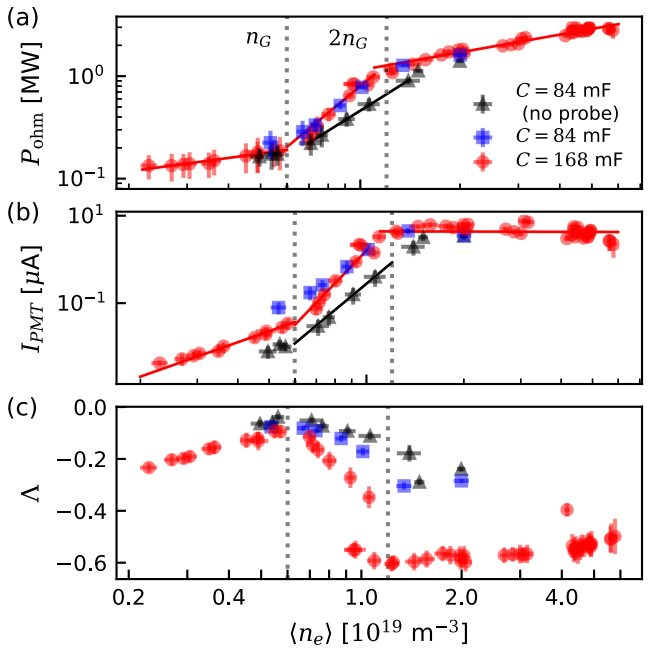

FIG. 3. Variation of (a) ohmic input power, (b) photomultiplier tube current from carbon III impurity line emission, and (c) poloidal asymmetry factor Λ with density in the range $f_G =$ 0.4 to 10, where $f_G = 1$ and 2, based on $I_p = 50$ kA, are indicated as dotted lines. Three datasets are shown with different power supply capacitance C, including one without probes inserted. Power-law fits to the data are shown in (a) and (b), as discussed in the text.

monochromator tuned to the carbon III 229 nm line, and panel (c) shows the poloidal asymmetry factor, $\Lambda = \tilde{b}_{\theta 1}(a) R_0 / a B_\theta = l_i/2 + \beta_p - 1$, where $\tilde{b}_{\theta 1}$ is the $m = 1$, $n = 0$ spatial Fourier component of the poloidal field B_θ at the plasma edge, $l_i = \langle B_\theta^2 \rangle / B_\theta^2(a)$ is the internal inductance, and $\beta_p = 2\mu_0 \langle p \rangle / B_\theta^2(a)$ is the mean plasma pressure normalized to the edge poloidal field. Smaller values of Λ correspond to flatter current profiles and/or lower thermal energy content. Three distinct regimes delineated roughly by $f_G = 1$ and 2 can be identified based on the scalings in Fig. 3, particularly in the more extensive $C = 168$ mF dataset. Power laws of the form $y \propto \langle n_e \rangle^x$ were fitted to data in Figs. 3(a) and 3(b), and the resulting exponents are given in Table I. The change in scaling around $f_G = 2$ is associated with an abrupt flattening of the toroidal current profile, based on the sharp decrease in Λ and internal probe measurements described below in the context of Fig. 4. The dataset with $C = 84$ mF (no probe) exhibits reduced radiation and input power and higher Λ, suggesting that further optimization could yield higher maximum density.

Prior measurements of core electron temperature, T_e, in MST tokamak plasmas with $f_G < 1$ yielded 60–70 eV [25]. Although direct measurement of T_e was not possible for the discharges presented here, rough estimates based on Spitzer resistivity, $\eta_{\rm sp} \propto T_e^{-3/2}$, and measured plasma resistance yield $T_e \sim 15$–20 eV for $f_G = 2$ and 5–10 eV for $f_G = 10$. This is consistent with an energy confinement time, τ_E, which decreases from about 1 to 0.1 ms over the range $1 < f_G < 10$. Additionally, internal probe measurements indicate that the current profile is constant in time starting at $t = 15$ ms or earlier. Therefore, the discharges are sustained much longer than the characteristic timescales for energy and current transport, so they are considered to be steady. Many of the proposed density limit mechanisms rely on turbulent or radiative energy losses from the plasma edge [10,12,20,21], so they are expected to develop on timescales comparable to τ_E.

Radiative power losses generally scale as $P \propto n_e n_Z L_Z(T_e)$, where n_Z is the density of ions with charge state Z, and L_Z is the radiative cooling rate [29]. For constant impurity content and temperature, radiated power $P_{\rm rad} \propto n_e^2$ is expected. For bremsstrahlung radiation due to electron-ion collisions, $L_Z(T_e) \propto T_e^{1/2}$, but it is more complicated when line radiation and recombination are included. For low-Z impurities, L_Z varies rapidly with T_e at low temperatures [30], which might explain the strong scaling of the carbon line radiation measurements in the

TABLE I. Power-law exponents from fits to separate datasets in Fig. 3 are given for specific ranges in f_G. The $C = 84$ mF dataset without probes is used.

Dataset	f_G range	$P_{\rm ohm}$ exponent	$I_{\rm PMT}$ exponent
$C = 168$ mF	< 1	0.43 ± 0.001	2.60 ± 0.02
$C = 168$ mF	[1, 1.6]	2.66 ± 0.13	7.63 ± 0.17
$C = 168$ mF	> 1.6	0.57 ± 0.001	-0.02 ± 0.01
$C = 84$ mF	[1, 2]	2.01 ± 0.001	6.16 ± 0.03

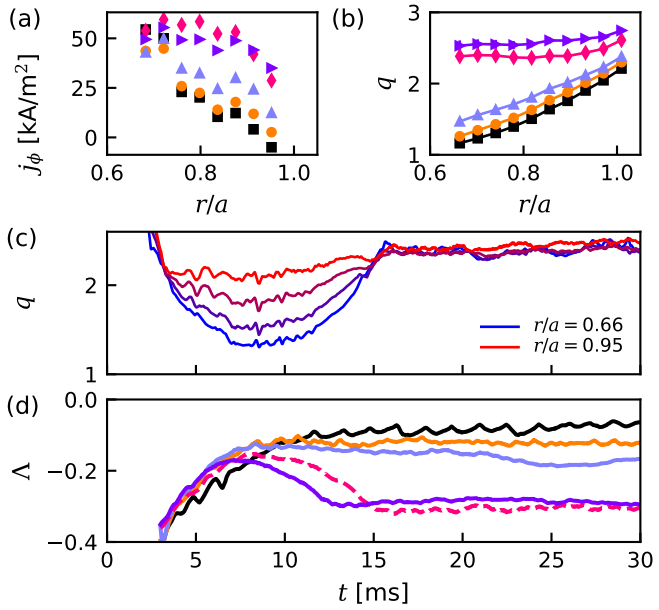

FIG. 4. Data from an internal magnetic probe showing (a) toroidal current profile and (b) safety factor profile for $0.65 < r/a < 1$ and $f_G = 0.87$ (black squares), 1.46 (orange circles), 1.74 (blue triangles), 3.46 (magenta diamonds), and 3.91 (purple triangles); (c) safety factor evolution from the probe at four radial locations for $f_G = 3.5$; and (d) evolution of the poloidal asymmetry factor, where colors correspond to the discharges in panels (a),(b), and the discharge in panel (c) is dashed.

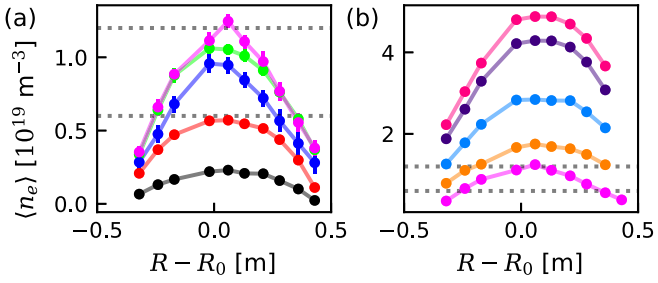

FIG. 5. Line-averaged electron density measured using an interferometer along 11 vertical chords at different major radii R are shown in the range (a) $0.4 \le f_G \le 2.1$ and (b) $2.1 \le f_G \le 8.1$. The data for $f_G = 2.1$ (magenta) are the same in both panels, and $f_G = 1$ and 2 based on $I_p = 50$ kA are shown as dotted lines.

range $1 < f_G < 2$. The radiated power fraction $P_{\rm rad}/P_{\rm ohm}$ was not measured, but if it is near unity then the power scaling in Table I for $1 < f_G < 2$ is roughly consistent with the expected n_e^2 dependence.

Further details of the current profile flattening implied by Fig. 3(c) are obtained from internal magnetic probe data, which are shown in Fig. 4 for $0.8 < f_G < 4$. At high f_G the current profile is finite out to the limiter, ruling out edge detachment. Interestingly, the $q(r)$ and $j_\phi(r)$ profiles do not change abruptly as $f_G = 1$ is crossed, but rather when f_G approaches 2. The current density rises near the wall, reaching a value $j_\phi \approx 50$ kA/m^2, which is close to $\langle j_\phi \rangle = 64$ kA/m^2 for $I_p = 50$ kA, implying a nearly flat current profile. The $q(r)$ profile also becomes flat, such that the low-order rational surfaces $q = 3/2$ and $2/1$ appear to be absent from the plasma. Probe and Λ measurements in Figs. 4(c) and 4(d) show that the flattening process occurs within about 5 ms early in the discharge. In most cases strong fluctuation activity is not observed. These may be global radiative collapse events [31], where radiative cooling drives up $L_Z(T_e)$, resulting in positive feedback and runaway cooling until a new equilibrium is reached with relatively weak gradients in $j_\phi(r)$ and $T_e(r)$.

Line-averaged density profiles measured by the 11-chord interferometer are shown in Fig. 5 for $0.4 \le f_G \le 8.1$, time-averaged over $20 < t < 30$ ms. In panel (a), the density profile broadens slightly with increased peak density up to $f_G = 1.8$ [green curve in Fig. 5(a)]. After the current profile flattens, the peak density drops slightly, and the density profile becomes more peaked (blue curve), indicating a change in particle confinement. Then, for $f_G > 3$ the profile once again broadens and shifts outboard (in the major radial direction). The outermost two chords in this direction are tangent to flux surfaces with $r/a \approx 0.69$ and 0.83, but the latter was not reliable for $f_G > 3$, probably due to beam refraction. Despite the lack of edge data, it appears that a density gradient is maintained across much of the profile at high density, in contrast with the flattened current profile that is affected by radiative losses.

Edge magnetic fluctuation measurements (not shown here) exhibit periodic bursts corresponding to sawtooth crashes below the Greenwald limit, transitioning to quasi-continuous, rotating tearing mode (TM) activity just above it. The TMs are generally weak or nonexistent after the current profile flattens near $f_G = 2$ since they are driven by the current gradient. However, in these conditions the magnetic shear is low, so pressure-driven modes are expected. It may be that interchange instabilities control particle transport above $f_G = 2$ while thermal transport is set by radiative processes, although this has yet to be confirmed. At the highest densities obtained, the ion collision frequency is near the cyclotron frequency, so the ions are expected to lose magnetic confinement while the electrons remain magnetized.

Questions remain about why, specifically, MST is able to operate with high Greenwald fraction, and to what extent this capability could be extended to higher-performance devices. The uniquely long resistive wall time and high-loop-voltage, feedback-controlled power supply are probably important. Notably, these features also permit stable operation of MST with $q(a) < 2$ [25]. The wall helps to stabilize RWM and TM that routinely cause disruptions in other devices. The observed changes to magnetohydrodynamic activity and power scaling above n_G support the idea that TM could play a role in setting the Greenwald

limit [10]. Further measurements are needed to properly assess the importance of interchange or ballooning turbulence [12,13,20,22]. The lack of edge current-profile collapse may be attributed to fast reaction of the active power supply to changes in plasma resistance. Since the supply is programmed to maintain constant I_p, radiative collapse of the core toroidal current is compensated by increased edge current drive and ohmic heating.

These results suggest that tokamak designs incorporating long resistive wall times and strong, versatile current-drive systems may be able to improve disruption resistance and/or permit routine operation above the density limit. The slow growth of RWM and TM due to the wall may allow control systems to maintain stable operation, or reduce thermal and magnetic quenching rates during disruptions. Collapse of the edge pressure and current profiles associated with density limit phenomena could be counteracted with advanced feedback current-drive and heating systems that can respond quickly and target the edge region.

Acknowledgments—We acknowledge expert technical assistance from Don Holly and the late Peter Weix. This work was supported by U.S. DOE Grant No. DE-SC0020245, by the Wisconsin Plasma Physics Laboratory (WiPPL), a research facility supported by the DOE Office of Fusion Energy Sciences under Contract No. DE-SC0018266, and by NSF Major Research Instrumentation Grant No. PHY 1828159.

[1] M. Murakami, J. D. Callen, and L. A. Berry, Nucl. Fusion **16**, 347 (1976).
[2] J. Hugill, Nucl. Fusion **23**, 331 (1983).
[3] M. Greenwald, J. L. Terry, S. M. Wolfe, S. Ejima, M. G. Bell, S. M. Kaye, and G. H. Neilson, Nucl. Fusion **28**, 2199 (1988).
[4] M. Greenwald, Plasma Phys. Control. Fusion **44**, 201 (2002).
[5] J. P. Freidberg, *Fusion Energy and Plasma Physics* (Cambridge University Press, Cambridge, England, 2007).
[6] M. Shimada, D. Campbell, V. Mukhovatov, M. Fujiwara, N. Kirneva, K. Lackner, M. Nagami, V. Pustovitov, N. Uckan, J. Wesley *et al.*, Nucl. Fusion **47**, S1 (2007).
[7] A. J. Creely, M. J. Greenwald, S. B. Ballinger, D. Brunner, J. Canik, J. Doody, T. Fülöp, D. T. Garnier, R. Granetz, T. K. Gray *et al.*, J. Plasma Phys. **86**, 865860502 (2020).
[8] J. W. Connor and S. You, Plasma Phys. Control. Fusion **44**, 121 (2002).
[9] G. Spizzo, P. Scarin, M. Agostini, A. Alfier, F. Auriemma, D. Bonfiglio, S. Cappello, A. Fassina, P. Franz, L. Piron *et al.*, Plasma Phys. Control. Fusion **52**, 095011 (2010).
[10] D. A. Gates and L. Delgado-Aparicio, Phys. Rev. Lett. **108**, 165004 (2012).
[11] R. B. White, D. A. Gates, and D. P. Brennan, Phys. Plasmas **22**, 022514 (2015).
[12] M. Giacomin, A. Pau, P. Ricci, O. Sauter, T. Eich, the ASDEX Upgrade team, JET Contributors, and the TCV team, Phys. Rev. Lett. **128**, 185003 (2022).
[13] P. Manz, T. Eich, and O. Grover, Nucl. Fusion **63**, 076026 (2023).
[14] D. Roberts, Nucl. Fusion **21**, 215 (1981).
[15] A. Gibson, Nucl. Fusion **16**, 546 (1976).
[16] J. Wesson, R. Gill, M. Hugon, F. Schüller, J. Snipes, D. Ward, D. Bartlett, D. Campbell, P. Duperrex, A. Edwards *et al.*, Nucl. Fusion **29**, 641 (1989).
[17] R. Maingi, M. Mahdavi, T. Petrie, L. Baylor, T. Jernigan, R. La Haye, A. Hyatt, M. Wade, J. Watkins, and D. Whyte, J. Nucl. Mater. **266–269**, 598 (1999).
[18] M. Bernert, T. Eich, A. Kallenbach, D. Carralero, A. Huber, P. T. Lang, S. Potzel, F. Reimold, J. Schweinzer, E. Viezzer, and H. Zohm, Plasma Phys. Control. Fusion **57**, 014038 (2015).
[19] Q. Teng, D. Brennan, L. Delgado-Aparicio, D. Gates, J. Swerdlow, and R. White, Nucl. Fusion **56**, 106001 (2016).
[20] B. N. Rogers, J. F. Drake, and A. Zeiler, Phys. Rev. Lett. **81**, 4396 (1998).
[21] R. Singh and P. Diamond, Nucl. Fusion **61**, 076009 (2021).
[22] T. Eich, P. Manz, and the ASDEX Upgrade team, Nucl. Fusion **61**, 086017 (2021).
[23] L. Giannone, R. Burhenn, K. McCormick, R. Brakel, Y. Feng, P. Grigull, Y. Igitkhanov, and the W7-AS Team, Plasma Phys. Control. Fusion **44**, 2149 (2002).
[24] R. N. Dexter, D. W. Kerst, T. W. Lovell, S. C. Prager, and J. C. Sprott, Fusion Technol. **19**, 131 (1991).
[25] N. C. Hurst, B. E. Chapman, A. F. Almagri, B. S. Cornille, S. Z. Kubala, K. J. McCollam, J. S. Sarff, C. R. Sovinec, J. K. Anderson, D. J. Den Hartog *et al.*, Phys. Plasmas **29**, 080704 (2022).
[26] H. R. Strauss, B. E. Chapman, and N. C. Hurst, Plasma Phys. Control. Fusion **65**, 084002 (2023).
[27] D. J. Holly, B. E. Chapman, K. J. McCollam, and J. C. Morin, in *Proceedings of the 2015 IEEE 26th Symposium on Fusion Engineering (SOFE)* (IEEE, New York, 2015), pp. 1–5.
[28] E. Parke, W. X. Ding, J. Duff, and D. L. Brower, Rev. Sci. Instrum. **87**, 11E115 (2016).
[29] J. Wesson, *Tokamaks*, 3rd ed. (Clarendon Press, Oxford, 2004).
[30] D. Post, R. Jensen, C. Tarter, W. Grasberger, and W. Lokke, At. Data Nucl. Data Tables **20**, 397 (1977).
[31] V. Ostuni, J. Morales, J.-F. Artaud, C. Bourdelle, P. Manas, N. Fedorczak, R. Dumont, M. Goniche, P. Maget, Y. Peysson, and the WEST Team, Nucl. Fusion **62**, 106034 (2022).